A Full-Scale Analysis of Absorption Edges in Dye-Doped Nonlinear Optical Polymers

Chen, Weilong; Zhang, Di; Zou, Jie; Luo, Jingdong

Published in:
Small Methods

Published: 20/11/2024

Document Version:
Final Published version, also known as Publisher's PDF, Publisher's Final version or Version of Record

Published version (DOI):
10.1002/smtd.202400162

Publication details:
Chen, W., Zhang, D., Zou, J., & Luo, J. (2024). A Full-Scale Analysis of Absorption Edges in Dye-Doped Nonlinear Optical Polymers. *Small Methods*, *8*(11), Article 2400162. https://doi.org/10.1002/smtd.202400162

small methods
www.small-methods.com

A Full-Scale Analysis of Absorption Edges in Dye-Doped Nonlinear Optical Polymers

*Weilong Chen, Di Zhang, Jie Zou, and Jingdong Luo**

A full-scale analysis of the absorption edges by modified Tauc-Lorentz models is essential in determining the optical bandgap and Urbach energy of semiconductors, transparent conductors, ionic compounds, and dielectric materials. This technique has not yet been applied to analyzing organic nonlinear optical (NLO) materials. This problem is tackled by preparing high-quality films of guest–host NLO polymers with a wide thickness range from sub-micron to 200 microns, allowing accurate measurement of full-spectral absorption coefficients of NLO materials over four orders of magnitude by the UV-VIS-NIR spectroscopy. The Tauc model and a new Monolog–Lorentz model are used to study the optical absorption edge of guest-host NLO polymers containing various push-pull chromophores and the dependence of optical bandgap and Urbach edge on the structure and composition of materials is analyzed. The results reveal the critical transition of the Urbach exponential tail to a low energy tail that overlaps with vibrational overtones of materials at the telecom wavelengths. Determining the fundamental absorption region of organic NLO films in this study provides quantitative insight into the research to harness the resonance-enhanced nonlinear coefficients of materials by operating at the wavelengths near the band edge with the control of optical loss.

1. Introduction

The research of organic second-order nonlinear optical (NLO) materials is now entering the fifth decade.[1–5] Thanks to the emerging nanophotonic and plasmonic platforms enabling strong light-matter interaction by orders of magnitude, the focused research efforts in organic electro-optic (EO) materials and hybrid devices are experiencing recent growth and considered to be a potential alternative to lithium niobate (LN) in ultrafast information processing for future 5G/6G technologies.[6–8] Ideal high-performance EO materials should possess large Pockels coefficients (r_{33} values),[9–12] high optical power handling (OPH), low optical loss (OL), fast response time, good thermal stability, and cost-effective processibility to interface with other materials.[13–16] Herein the n^3r_{33} values determine the half-wave voltage (V_π) of waveguide modulators, where n is the refractive index of EO materials, and high OPH and low OL are essential to achieve high optical output power (P_L).[17] As a primary figure of radio-frequency (RF) photonic link, overall RF power gain (G) of waveguide modulators is given by [18]

$$G \propto \left(\frac{P_L}{V_\pi}\right)^2 \propto \left(\frac{n^3 r_{33}}{OL}\right)^2 \quad (1)$$

At a given interaction length of waveguides, it dictates EO materials' figure of merit (FOM) as $(n^3r_{33}/OL)^2$ for achieving high G, instead of the r_{33} values alone. The past two decades have witnessed considerable research progress in the design and synthesis of organic EO (OEO) materials exhibiting large r_{33} values for low V_π modulators, as well as improved thermal stability of poled films.[9–16] Equally important but rarely addressed in the development of OEO materials is to achieve low optical loss at the operational wavelengths of telecom C-band (1530–1565 nm) for long-haul communications and O-band (1260–1310 nm) for data center interconnects, which are extremely important for achieving high OPH and low OL to enable high P_L in waveguides.[9a,14,17] Due to relatively high optical loss, OEO materials, including EO polymers and dendrimers, show a critical disadvantage of FOM of $(n^3r_{33}/OL)^2$ in comparison with those from commercial LN (Table S1, Supporting Information).[19]

In general, highly active OEO materials exhibit strong near-infrared (NIR) optical absorption from push-pull polymethine or polyene chromophores. The strong NIR absorption of chromophores is essential for achieving large molecular hyperpolarizabilities (β_{EO}). Also, it may offer a unique opportunity to

W. Chen, D. Zhang, J. Zou, J. Luo
Department of Chemistry
City University of Hong Kong
Hong Kong SAR 999077, China
E-mail: jingdluo@cityu.edu.hk
W. Chen, D. Zhang, J. Zou, J. Luo
Shenzhen Research Institute
City University of Hong Kong
Shenzhen 518057, China
D. Zhang, J. Luo
Hong Kong Institute for Clean Energy
City University of Hong Kong
Hong Kong SAR 999077, China

The ORCID identification number(s) for the author(s) of this article can be found under https://doi.org/10.1002/smtd.202400162

DOI: 10.1002/smtd.202400162

maximize the NLO activities of OEO materials by operating at the wavelengths near the absorption edge, should the waveguides OL be within control.[17,20] Nevertheless, there are few studies and/or limited data on how the NIR absorption of push-pull chromophores, typically ranging from 700 to 1200 nm, can affect the OL of OEO materials at the operational long wavelengths around 1300 and 1550 nm. This work is to verify the optical loss of the current EO polymers. The optical band gap and Urbach energy of these new materials have not been systematically analyzed from any prior research. The difficulty is mainly due to large change of absorption coefficients over different orders of magnitude for the materials.

Previously Barto et al. have combined the UV–VIS–NIR transmission spectroscopy and photothermal deflection spectroscopy (PDS) to characterize the continuous spectrum from high energy and strong dye electronic transition peak in the VIS-NIR region up to 1100 nm to the weak absorption in the telecom NIR region up to 1830 nm.[21,22] The studies have gained important insights into the mechanisms, such as continuum dielectric effects in polycarbonate hosts and bonding/molecular environment effects, responsible for NIR loss in the early generation of EO polymers. The PDS technique has been considered as one of the most sensitive methods for measuring extremely weak absorptions from vibrational overtones and tail states from the main electronic absorption peak of chromophores. However, unlike the UV-VIS-NIR spectroscopy, PDS has not been widely implemented as a commercial tool for the analysis of weak absorptions, mainly due to its indirect measurement principle, sophisticated experimental configuration, and time-consuming data analysis. In addition, commercial spectroscopic ellipsometry has the measurement accuracy of extinction coefficient (k) at 0.001, which is still orders higher than the values from weak absorptions of optical polymers.[20] Other commonly used method, such as the waveguide cut-back method, is fast and straightforward. However, the accuracy of this method is limited because it is difficult to maintain uniform facet quality and coupling efficiency during every measurement after cutting the waveguide.

Therefore, it is imperative to develop new techniques to allow accurate measurement of full-spectral absorption coefficients of OEO materials from strongly absorbing VIS-NIR electronic transitions to weak absorption bands of vibrational overtones and electronic tail states. Recently, Yamada et al. have used the UV-VIS-NIR spectroscopy to measure both the strong absorption from electronic excitation in thin films and the weak absorption from the tail states and overtones in thick films of EO polymers, in which the structure of chromophores is based on the dialkylamino-substituted thiophene stilbenes with the tricyanovinyldihydrofuran (TCF) acceptors.[23] The study has identified the critical trade-off between the absorption loss, photostability, and r_{33} values at the O-band. Similarly, we tackle this important problem in this study by developing new processing protocols to prepare high-quality films of guest-host NLO polymers with a wide thickness range from sub-micron to 200 microns, which allows accurate measurement of full-spectral absorption coefficients of NLO materials over four orders of magnitude (1–10^4 cm^{-1}) by UV-VIS-NIR spectroscopy. In particular, we study the optical absorption edge of guest–host NLO polymers containing a variety of push-pull chromophores by Tauc fitting and analyze the dependence of optical band gap and Urbach edge on the structure and composition of materials.

Based on the energy dependence of the absorption over the band gap, the Tauc method has been established to characterize the optical band gap for semiconductors.[24,25] The disorder in the crystals would broaden band edges of localized states, which could extend into the pseudogap.[26] These localized states originate from weak bonds that correspond to deviations from the ideal bond length and bond angle.[27] The absorption edge could be divided into three regions (see Note S1, Supporting Information): Region A (Tauc plot for determining the optical band gap,[24] **Figure 1**a,b), Region B for Urbach edge, and Region C for low-energy tail [28] (Figure 1b).

The simple Tauc model does not consider electronic transitions between disorder-induced tail states and extended states. In recent years, more accurate models have been established to identify the optical band gap (E_G) and Urbach energy (E_U), and a commonly used dispersion model is the Tauc-Lorentz (TL) model with different modifications.[27b,29] In particular, a simplified Monolog–Lorentz (ML) model has been developed by Guerra et al. to analyze the fundamental absorption along with the Urbach region (see Note S2, Supporting Information). It allows the determination of the E_G and E_U of the materials from a single fit of the absorption spectra, without the need to differentiate the Tauc and Urbach regions beforehand.

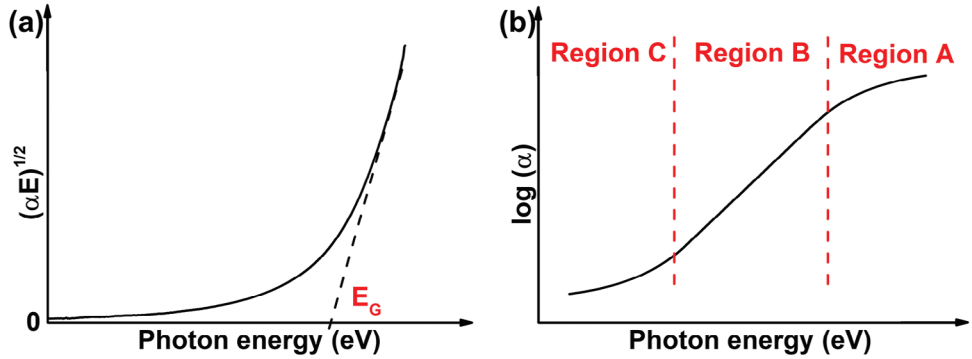

Figure 1. a) Example of a Tauc plot for the analysis of absorption spectra to fit the linear region to evaluate E_G at the x-axis intercept as the optical band gap of the material (α is the absorption coefficient and E is the photon energy in eV); b) Distinguished three regions based on the different response to the absorption coefficient.

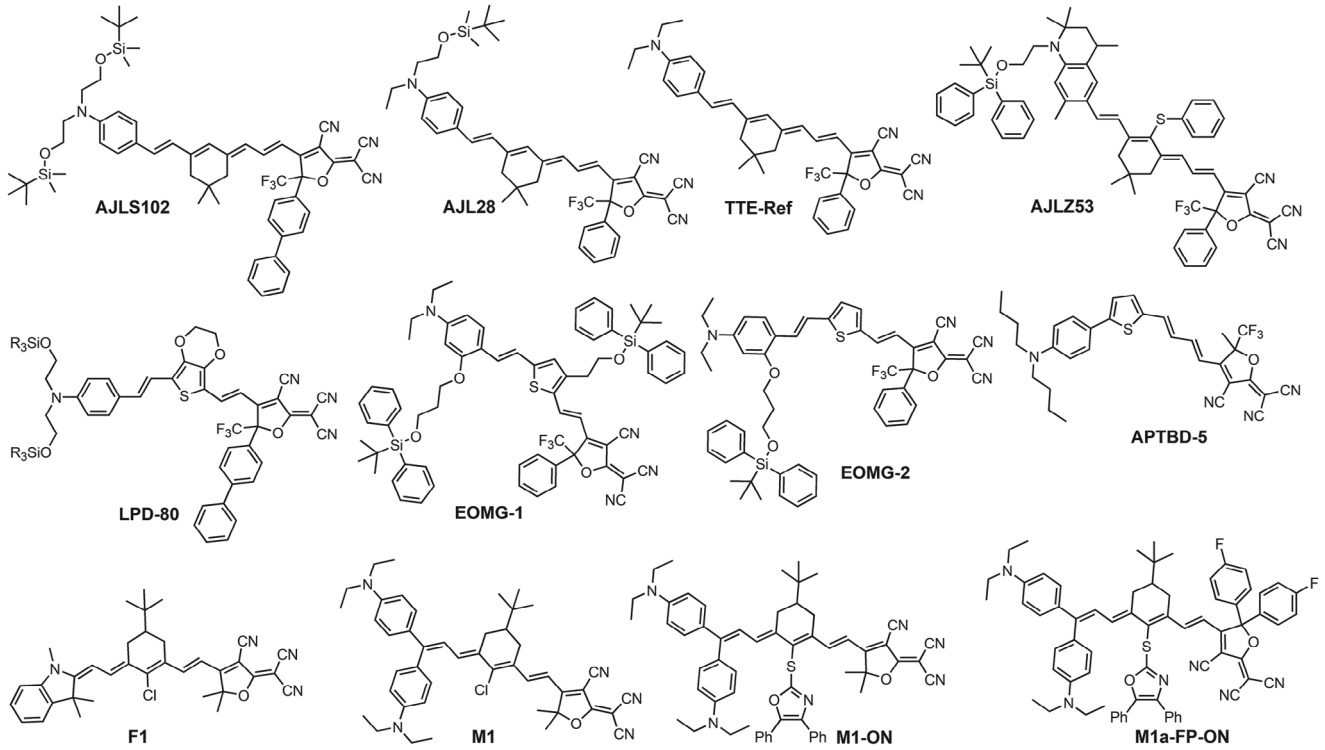

Figure 2. Molecular structures of three types of TCF-based push-pull chromophores containing different conjugated π-systems of phenyltetraenes, thiophene stilbenes, and heptamethines, respectively.

To the best of our knowledge, there is no previous report on the determination of the optical band gap and Urbach energy from optical absorption measurements of OEO materials. This study aims to address this gap by investigating the structure-property relationships of 12 high-activity push-pull chromophores (**Figure 2**) through the Tauc model and the simplified ML model. To achieve this, high-quality films of guest–host NLO polymers containing these chromophores were prepared through solution processing. The film thicknesses were controlled to range from sub-micron to 200 microns, allowing for the measurement of the full VIS-NIR spectra of films, including strong electronic transitions to weak absorption bands of vibrational overtones and electronic tail states. The ability to measure the absorption coefficients of OEO materials, which varied several orders of magnitude from 1 to 10^4 cm^{-1}, enabled us to conduct the curve fitting to analyze the dependence of the optical band gap and Urbach edge on the structure and composition of OEO materials.

2. Results and Discussion

2.1. Preparation of Thin Films and Thick Slabs

To obtain the full-spectral absorption coefficients of NLO materials over orders of magnitude by the common UV-VIS-NIR spectroscopy, first, we need to prepare high-quality OEO films with thicknesses ranging from sub-micron to a few hundred microns. While it is common that thin film samples of guest-host EO polymers can be easily prepared by spin-coating for the measurement of the strong absorption of electronic excitation with the α up to 10^4 cm^{-1}, the preparation of thicker samples requires different protocols to build up sufficient absorbance for the reliable measurement of weak absorptions with α down to 1 cm^{-1}. We have modified the protocol of drop-casting, followed by hot-embossing, previously developed in the study of organic photorefractive (PR) materials, to prepare high-quality void-free thick films of guest–host EO polymers (**Figure 3**). To do this, we first prepared a hydrophobic glass slide as the top contact by functionalizing a well-defined self-assembled monolayer (SAM) through the reaction of *n*-octyltrichlorosilane (OTS) with the hydroxyls of the activated glass surface (Figure 3a). Second, we took the commercial PTFE printed microscope slide containing a round well with a diameter of 8.0 mm for drop-casting, and the amounts of materials were controlled to meet the range of thicknesses. The PTFE-printed slides are extremely hydrophobic, solvent-resistant, chemical resistant, and perfect for controlling cross-contamination for drop-casting. Also, it can reduce the unevenness for more efficient hot-embossing. The well surface is 100% wettable to enhance film adhesion and increase its spreading capabilities. Overall, the use of these slides greatly minimized the use of precious formulated EO polymer solutions. Then, the drop-casted films were allowed to stand overnight for slow evaporation of solvents to form relatively flossy, dense, but still uneven slabs well within the well. Finally, the prepared slabs were covered with the OTS-treated glass slide and inserted into a hot press machine with a polyimide spacer. The samples were heated to an elevated temperature, typically 20–30 °C above the glass transition temperatures of EO polymers, and kept for a few

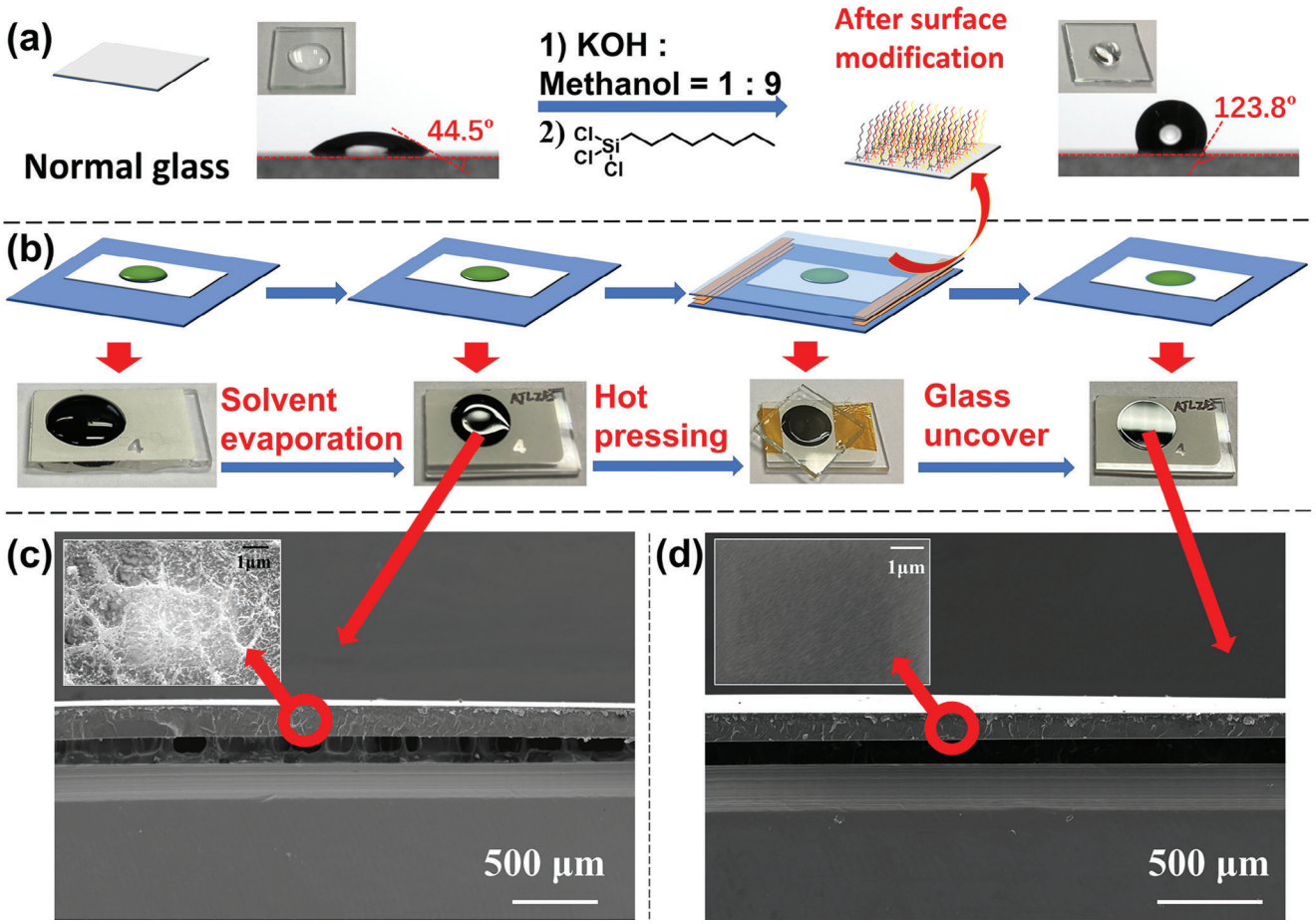

Figure 3. a) Schematic diagram showing the difference of contact angle after the surface modification; b) Schematic illustration of processing followed by drop casting and hot pressing to obtain thick slabs with high optical quality; c) Cross-section SEM images of guest–host polymeric films after drop casting with the observation scale of 1 micron and 500 microns; d) Cross-section SEM images of guest–host polymeric films after hot-pressing with the observation scale of 1 and 500 microns.

minutes (Figure 3b). The pressed samples were allowed to cool to the ambient temperature and smooth films with exceptionally high optical quality and free of voids were obtained with controlled thicknesses (Figure 3c). Due to the presence of OTS-SAM, the top cover glass slide can be easily peeled off from the films, and the films (Figure 3d) were used for the measurements of thicknesses and UV-VIS-NIR spectra.

The solutions of EO polymers were formulated by mixing the solid of host polymers and chromophores in dibromomethane (DBM) at two given solid concentrations of 3.0 and 6.0 wt.%. Two commercial optical polymers, namely poly (styrene-*co*-methyl methacrylate) (PSM) and a cyclic olefin polymer (COP), were selected due to their excellent optical and dielectric properties, good compatibility with TCF-based push-pull chromophores, and efficient film preparation by spin-coating for thin films and hot embossing for thick slabs on the glass substrate. Other commonly optical polymers, including poly(methyl methacrylate) (PMMA), poly(bisphenol A carbonate) (PC), and polyetherimide, were not included due to the requirement of very high temperatures greater than 200 °C for hot embossing that was beyond typical thermal decomposition temperatures of chromophores. The spin-coated thin films of formulated materials, with a thickness from ~400 to ~1200 nm by the DektakXT Stylus Profiler, were used for the measurement of VIS-NIR spectra to evaluate the Region A exhibiting ultrahigh absorption coefficients, typically in the range of 10^3–10^4 cm^{-1}.[31] To prepare thick slabs, the amount of solution in drop-casting and the solution concentration can easily control the thickness range. A series of optical quality slabs with thicknesses ranging from ~50 to ~250 μm were prepared and used for the measurements of VIS-NIR spectra to evaluate the low absorption regions of materials with absorption coefficients in the range from 1.0 to 100 cm^{-1}.[32]

2.2. Absorption Spectra of the Host Polymers

The absorption of the pure polymeric matrix is first confirmed by NIR vibrational overtones arising from anharmonicity, such as C-H, O-H, and N-H stretches.[33,34] These overtones are extremely weak and cannot be detected by conventional reflectance or transmission techniques. Susceptible methods like photoacoustic and photothermal deflection spectroscopy are commonly employed to verify these transitions.[35–37] However, such weak transitions

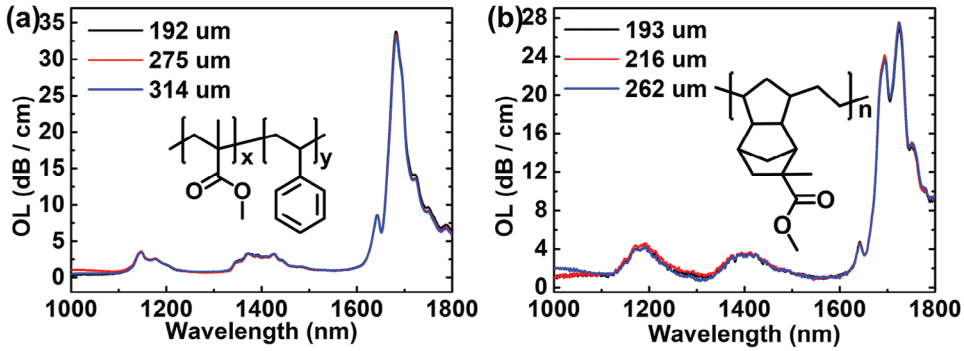

Figure 4. UV–VIS–NIR absorption loss spectra for pure polymeric materials. Shown are the data for PSM with varied thicknesses a) and COP with distinct thicknesses b). (Standard Deviation (SD) for α: 0.035 cm^{-1} for PSM and 0.021 cm^{-1} for COP).

in the NIR region can be measurable to a high level of fidelity by increasing the thickness of the measured slabs. The extended optical path may allow the weak absorbance to be quantified by rapid measurements in commercial UV–VIS–NIR transmission spectroscopy.

The relevant overtone absorptions of PSM and COP in the NIR range (1000–1800 nm) are initially examined by altering the thickness of the polymeric slabs. As illustrated in **Figure** 4a, the NIR spectra of the PSM with distinct thickness are comprised of three peaks, a modest C-H stretching overtone centered at ~1140 nm, a weak C-H stretching-plus-bending combination overtone centered at ~1400 nm, and a strong C-H stretching overtone at ~1680 nm. The C-H overtones at 1140, 1400, and 1680 nm are insensitive to the thickness of slabs, indicating that the overall concentration of C-H moieties is relatively constant. For the NIR spectra of the COP in Figure 4b, the different C-H stretching vibrations are characterized by the two firm overtone peaks at 1694 and 1724 nm, which may correspond with different molecular structures. Both PSM and COP exhibit minimum OL (less than 1 dB cm^{-1}) at three major operational wavelengths of 1.06, 1.3, and 1.55 μm, which lie between the C-H vibrations. The OL values are comparable with the data from the PDS and the prism-coupling method in slab waveguides.[38]

2.3. Loading-Density-Dependent Analysis

We selected two highly soluble chromophores AJLZ53 and LPD-80 [39] to study the optical absorption of formulated guest–host polymers as a function of chromophoric loading density (N). A UV–VIS–NIR absorption spectrum scanning from 400 to 1800 nm in transmission mode is collected through the different regions of overlap between varied films with distinct thicknesses to complete the full-range optical absorption spectrum. Figure S1 (Supporting Information) illustrates the collection and mathematical treatments of the various measured regions of the AJLZ53-doped PSM slabs based on the Tauc model (hereafter AJLZ53@PSM). **Figure** 5a shows a representative AJLZ53@PSM spectral overlay with increasing N from 0.60×10^{20} to 1.30×10^{20} cm^{-3}. For AJLZ53-based guest–host systems, the spectra consist of two peaks from a strong dye π–π^* electronic transition around 835 nm and a modest C-H stretching overtone near 1680 nm. The two characteristic overtone peaks of PSM at 1140 and 1400 nm are covered by the extended absorption edge of AJLZ53. The major peak in the visible region displays a linear rise with the increasing N, as predicted by the Beer-Lambert Law. The intensity of the second peak in the NIR region, which comes from the C-H stretching overtones, does not vary as N varies. The overtone-based behavior indicates that the overall concentration of C-H moieties in the guest–host system is not significantly altered by the loading density of chromophores.

In Table S2 (Supporting Information), the Tauc analysis of AJLZ53@PSM guest–host systems shows that increasing chromophores loading density causes E_G red-shifted, from 1.105 eV at N of 0.60×10^{20} cm^{-3}, to 1.089 eV at N of 0.94×10^{20} cm^{-3}, to 1.069 eV at N of 1.30×10^{20} cm^{-3}, respectively. The simplified ML model shows a similar trend of redshift from 1.168 to 1.126 eV in the obtained E_G. The broadening behavior of the dye electronic absorption peak can be associated with the dye orientations caused by the dye-dye and dye-polymer interactions. It is determined that the overall broadening behavior of guest–host polymers increases the optical loss at 1.3 μm of 26.0, 50.5, and 93.1 dB cm^{-1} at N of 0.60×10^{20} , 0.94×10^{20}, and 1.30×10^{20} cm^{-3}, respectively (see Figure S2a, Supporting Information). As shown in Figure 5c, E_U can be calculated from the slope of the straight line plotting $\ln(\alpha)$ against the incident photon energy ($h\nu$) or the nonlinear fitting of the simplified ML model. Here E_U, which is below the band gap energy, characterizes the width of the exponential distribution. The Urbach width has a thermal contribution, and contributions from temperature-independent disorder and distribution of defects in the material.[40,41] For the amorphous guest–host polymer, the Urbach tail broadening is one of the significant contributions to the NIR loss.[42] For the Tauc analysis in Table S3 (Supporting Information), the Urbach energies at 10 $cm^{-1} < \alpha < 100$ cm^{-1} significantly increase from 36.0 meV for the N of 0.60×10^{20} cm^{-3}, to 47.8 meV for the N of 0.94×10^{20} cm^{-3}, and to 57.8 meV for the N of 1.30×10^{20} cm^{-3}, respectively. However, the E_U at higher absorption coefficients varies slightly from 28.2 meV at the N of 0.60×10^{20} cm^{-3}, to 29.0 meV at the N of 0.94×10^{20} cm^{-3}, and to 30.1 meV at N of 1.30×10^{20} cm^{-3} (see Figure S2b, Supporting Information). For the simplified ML model, the E_U stays nearly unchanged, indicating that the Urbach energy is the intrinsic characteristic of chromophores. The comparison between these two models shows that the Urbach energy determined by the Tauc

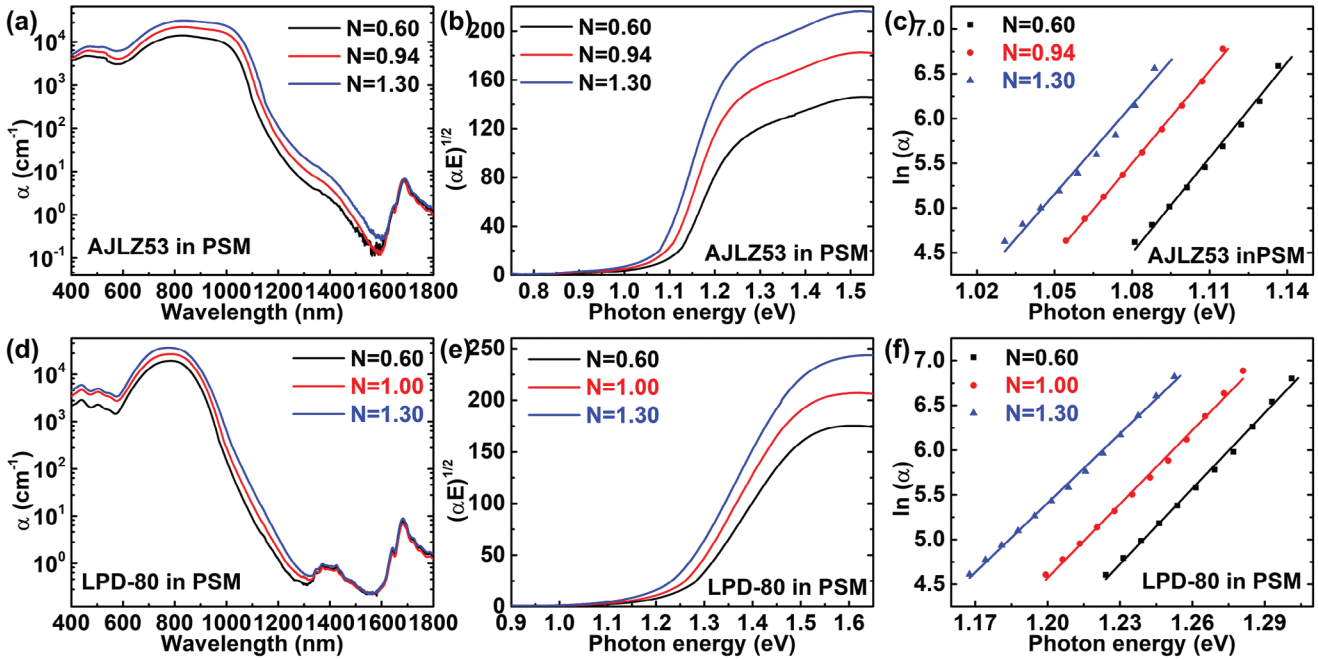

Figure 5. a) Absorption coefficient plot of AJLZ53@PSM polymeric films with distinct *N* at the range of 400–1800 nm; b) Tauc plot of AJLZ53@PSM polymeric films with distinct *N*; c) Urbach edge analysis by the Tauc method at low absorption coefficient region of AJLZ53@PSM polymeric films with distinct *N*; d) Absorption coefficient plot of LPD-80@PSM polymeric films with distinct *N* at the range of 400–1800 nm; e) Tauc plot of LPD-80@PSM polymeric films with distinct *N*; f) Urbach edge analysis by Tauc method at low absorption coefficient region of LPD-80@PSM polymeric films with distinct *N*. The unit for *N* is 10^{20} cm^{-3}.

method in the lower energy, especially for guest–host polymers containing the most red-shifted chromophore, might be significantly dependent on the bias induced by the exponential tails in the Tauc-scale absorption. The increment in the red-shifted band gap and the rising of OL indicates that simply raising the *N* of guest chromophores may not be beneficial in reducing the OL of materials.

The LPD-80@PSM guest–host films are also subjected to loading-dependent analysis. As is shown in Figure 5d, which is different from the AJLZ53@PSM system, three peaks are shown in the spectra of absorption coefficient, including a strong dye π-π* electronic transition at 785 nm, a C-H stretching-plus-bending combination overtone at 1400 nm, and a modest C–H stretching overtone at around 1680 nm. The emergence of the peak at 1400 nm, which originates from the overtones of pure PSM, is primarily due to the blue shift of π-π* electronic transition. The blue-shifted chromophoric absorption edges lead to relatively low optical losses of LPD-80@PSM films. As the *N* increases, OLs at 1.3 μm slightly rise from 1.6 to 2.6dB cm^{-1} (see Figure S2c, Supporting Information). Similarly, the intensity of overtone absorption at the NIR region does not change much with *N*, indicating weak dependence on the chromophore concentration. The intensity change of π-π* electronic transition follows the Beer-Lambert Law. Table S4 (Supporting Information) depicts similar trends on redshifted E_G based on the Tauc and simplified ML models. For the Urbach energy analysis, Figure 5f, Figure S2d, and Table S2 (Supporting Information) support that E_U will not be affected by the loading density of the chromophores in the guest–host polymers. The comparison of the AJLZ53@PSM and the LPD-80@PSM shows that the distinct molecular structures of guest chromophores would create distinctly different absorption edges in thin films. The bent structure of the π-conjugation bridge in the thiophene stilbene-based chromophore LPD-80 results in a blue-shifted π-π* electronic transition of the chromophore, leading to lower OL and larger Urbach energy in comparison to straight push-pull phenyltetraene chromophores such as AJLZ53.

2.4. Chromophore-Structure-Dependent Analysis

The link between the chemical structure of dyes and the absorption edge of guest–host films is investigated using three series of standard push-pull chromophores (**Figure 6** and **Table 1**). The TTE-Ref chromophore has the simplest push-pull structure without additional steric modification, leading to a red-shifted band gap and a large optical loss of 52.9 dB cm^{-1} at 1.3 μm. Its high OL may be contributed in part by light scattering from chromophore aggregates. In comparison, by introducing one *tert*-butyldimethylsilane group to the donor part, AJL28 achieves a larger band gap and a lower optical loss of 21.1 dB cm^{-1} at 1.3 μm. For the AJLS102 with two bulky *tert*-butyldimethylsilane groups in the donor part and a biphenyl group in the acceptor, its Urbach energy increases substantially with a larger band gap, likely due to reduced dipole-dipole interaction of chromophores. Overall, we find that tuning the donor strength of the chromophores can blue-shift the absorption band of electronic transition to effectively reduce the OL of guest-host polymers, while not significantly

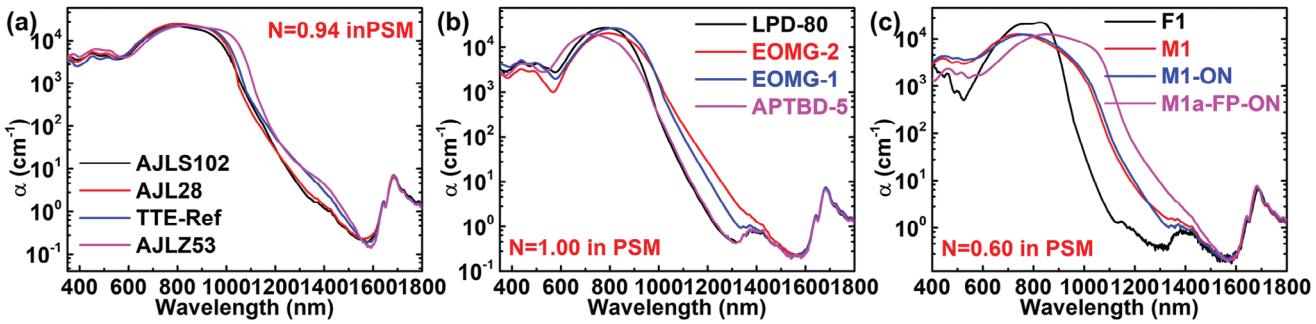

Figure 6. a) Absorption coefficient of phenyltetraenes@PSM including AJLS102, AJL28, TTR-Ref, and AJLZ53; b) Absorption coefficient of thiophene stilbenes@PSM including LPD-80, EOMG-2, EOMG-1, and APTBD-5; c) Absorption coefficient of heptamethines@PSM including F1, M1, M1-ON, M1a-FP-ON. The unit for N is 10^{20} cm^{-3}.

compromising the molecular hyperpolarizabilities (Table S4, Supporting Information).

For the thiophene stilbene-based series, nearly all guest–host films showed three main absorption peaks including an overtone band centered at 1400 nm, except for the EOMG-2@PSM that displayed the most red-shifted absorption edge in the series (Figure 6b). The OLs of the thiophene-stilbene-based chromophores at 1.3 μm are much lower than those of the phenyltetraene-based chromophores in guest–host polymers. For the guest–host polymers based on EOMG-1 and EOMG-2, introducing one more bulky group to the push–pull structure of the chromophores leads to higher E_G and E_U. Meanwhile, OLs at 1.3 μm rise from 6.6 dB cm^{-1} for EOMG-1-based polymer to 19.4 dB cm^{-1} for EOMG-2-based one, underscoring the critical role of steric modification to the chromophore structures. It is worth noting that the unique chromophore APTBD-5 [43] in our previous work exhibits reasonable Urbach energy and low optical loss in these types of thiophene stilbene-based polymers, which deserves in-depth investigation on achieving trade-off between large nonlinearity and low loss.

Figure 6c shows the absorption spectra of the push-pull heptamethine-based series. As the newly developed chromophores, the Michler-base-type chromophores such as M1, M1-ON, and M1a-FP-ON exhibit excellent NLO performance. According to Table 1 and Figure S5 (Supporting Information), we find that:

1) The mercapto substitution by the 4,5-diphenyl-oxazol-2-ylsulfanyl group in M1-ON will slightly redshift the chromophore absorption band in the PSM, resulting in the slightly smaller EG, larger EU, and lower OL compared with M1-based polymer. However, the EO coefficient of M1-ON-based polymer increases to 141% compared with that of M1-based polymer, implying that appropriate thioether substitution would be one applicable method to enhance EO performance and maintain the low OL simultaneously.[44]
2) M1a-FP-ON, one of the most reshifted heptamethines, shows comparable E_G, E_U, and OL with AJLZ53 in PSM, even at a low N of 0.60 × 10^{20} cm^{-3}. In prior work, M1a-FP-ON exhibits an ultralarge β_{EO} value of 8437 × 10^{-30} esu at 1.3 μm, exceeding the result of AJLZ53.[44] Nevertheless, the present

Table 1. Summary of band gap energy (E_G), Urbach energy (E_U), and optical loss of chromophores with different N in PSM.

	N [×10^{20} cm^{-3}]	ML model		Tauc model		Optical loss at 1300 nm [dB/cm]
		E_G [eV]	E_U [meV]	E_G [eV]	E_U [a)] [meV]	
AJLS102	0.94	1.217	62.6	1.140	41.6	16.7
AJL28	0.94	1.200	48.0	1.129	42.6	21.1
TTE-Ref	0.94	1.197	42.1	1.121	44.6	52.9
AJLZ53	0.94	1.147	50.7	1.089	29.0	51.9
LPD-80	1.00	1.309	58.1	1.237	36.4	2.2
EOMG-2	1.00	1.270	80.6	1.149	51.4	19.4
EOMG-1	1.00	1.296	69.3	1.182	43.6	6.6
APTBD-5	1.00	1.284	66.8	1.221	45.0	2.1
F1	0.60	1.467	52.2	1.310	26.8	1.9
M1	0.60	1.139	43.6	1.128	32.5	8.8
M1-ON	0.60	1.133	45.4	1.118	33.5	6.7
M1a-FP-ON	0.60	1.079	35.2	1.064	27.1	39.8

[a)] The E_U values determined by the Tauc model in the above table are in the high Urbach region with α ranging from 100 to 1000 cm^{-1}.

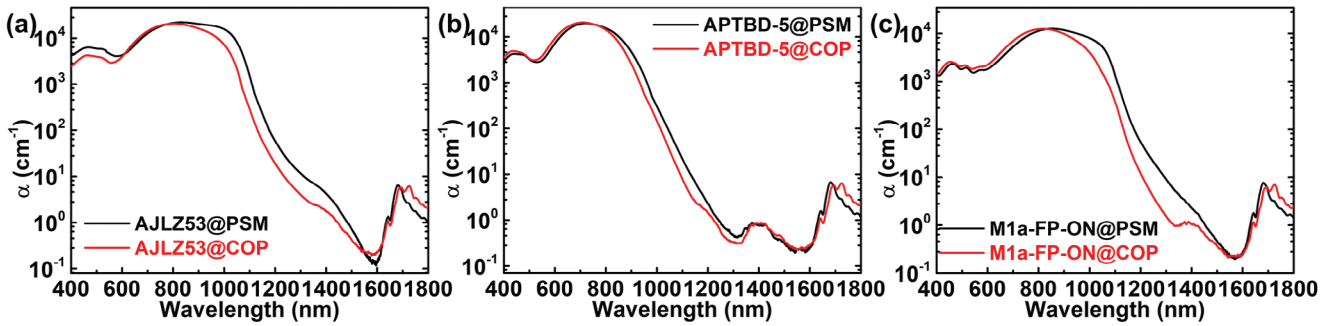

Figure 7. a) Absorption coefficient of AJLZ53@PSM and AJLZ53@COP with $n = 0.94 \times 10^{20}$ cm^{-3}; b) Absorption coefficient of APTBD-5@PSM and APTBD-5@PSM with $n = 1.00 \times 10^{20}$ cm^{-3}; c) Absorption coefficient of M1FPON@PSM and M1a-FP-ON@PSM with $n = 0.60 \times 10^{20}$ cm^{-3}.

study indicates that the M1a-FP-ON@PSM would induce a much higher loss at the same loading density than those of AJLZ53@PSM. Thus, molecular modification would be needed to reduce the OL due to chromophore absorption tails.

3) Even though the F1-based polymer has a minimal EO coefficient due to its cyanine-like electronic structure, this narrow band shape makes the overtone peak centered at 1140 and 1400 nm showing up, providing the guest–host polymer with a broad optical transparent window in the NIR region.[45] According to Marder's prediction, one can potentially exploit near-resonance enhancement of the real part of the molecular third-order polarizability $Re(\gamma_0)$ without incurring a significant optical loss, which offers the potential for the investigation of the new NLO chromophores with large $Re(\gamma_0)$ and low OL.[20a,46]
4) The push-pull heptamethines showed smaller E_U values than those of phenyltetraene and thiophene stilbene-based chromophores. As a smaller E_U corresponds to a slower decreasing slope of optical absorption in the Urbach tail, this feature may not be desirable to achieve broad transparency windows in the NIR regions and the underlying mechanisms deserve further investigation.

2.5. Host Polymer-Dependent Analysis

Because polymers have distinct polarity and variable compatibility with dipolar chromophores, the guest–host films based on PSM and COP exhibit quite different optical absorption. Figure S6 (Supporting Information) depicts the dielectric constants of PSM and COP at different frequencies, revealing that PSM is more polar than COP. **Figure** 7a depicts the absorption edge of AJLZ53 in PSM and COP. The strong π-π* electronic transition peak shifts from 835 nm to 795 nm when the polymer matrix changes from PSM to COP, which has a lower polarity. The π-π* electronic transition peaks of polymers based on APTBD-5 and M1a-FP-ON in Figure 7b,c show similar blueshifts and lower OLs in less polar host polymer of COP. As shown in Table S5 (Supporting Information), the optical loss at 1.3 μm of AJLZ53-based polymers falls from 50.5 dB/cm for PSM to 17.4 dB cm^{-1} for COP. Similar changes are found for APTBD-5 and M1a-FP-ON.

Table S6 (Supporting Information) illustrates the distinct Urbach energy in the different absorption scales by the Tauc method. Compared with the results from the simplified ML model, the Urbach energy determined by the Tauc method at the lower absorptional region with α from 10 to 100 cm^{-1} indicates that the absorption edge smearing at a low absorptional area would be strongly affected by the overtones of the host polymers. Thus the simplified ML model and Tauc analysis at higher absorptional region are used to obtain the reasonable Urbach energy. For these three series of chromophores, the larger Urbach energy in PSM over COP may be affected by the compatibility of guest-host systems.

3. Conclusion

We report the systematic full-scale analysis and the structure-property relationship study of the optical absorption edge of guest–host polymer films to investigate their optical losses. High-quality films of guest–host NLO polymers with thicknesses ranging from sub-micron to 200 microns are produced using spin coating or drop-casting methods. The full-range absorption spectra spanning several orders of magnitude from 1 to 10^4 cm^{-1} are captured across several regions. Three series of EO chromophores are utilized to carry on the thickness-dependent, loading density-dependent, dye structure-dependent, and host polymer-dependent analysis to investigate the absorption behavior in distinct host polymers.

The Tauc method and the simplified ML model were applied to analyze the optical band gap and Urbach energy on the different guest–host polymers. The analysis is informative for possible strategies to lower the optical loss of EO polymers. The increasing loading density of chromophores in the guest–host system reasonably improves the EO coefficients, but the red-shifted band gap could unavoidably raise the optical loss of the materials. Introducing bulky modification groups to the chromophore structures will efficiently increase the Urbach energy of materials, which is probably due to the reduction of the dipole-dipole interactions between chromophores in the polymer. For those polymers with relatively small Urbach energies, lowering the polarities of the host polymers is one facile method to reduce the optical losses of materials.

As our study has demonstrated the measurements and optical dispersion analysis of full-spectral absorption of new EO polymers in the NIR region, future studies should be focused on the poled EO films and vigorous development of new semi-empirical

optical dispersion models that can consider the exceptional optical anisotropy and near-band-edge feature of organic EO materials. We expect that such endeavors could go a long way to achieve both high EO activity and low optical loss in the critical development of high-performance organic EO materials for photonic applications.

4. Experimental Section

Materials: All the chemicals and reagents were used as received. OTS and DBM were purchased from Sigma Aldrich. The "PTFE" printed slides were purchased from Electron Microscopy Sciences.

Contact Angle Measurement: Contact angle was measured with an optical tensiometer (SL200KS). A drop of liquid water was placed on the surface of the sample of interest and the contact angle was calculated by Program CAST3.0.

Scanning Electron Microscopy: To observe the cross-section morphology of the EO films before and after the hot-embossing, a scanning electron microscope (Philips XL30 ESEM) was used to visualize the morphology at different scales (500 and 1 μm).

UV-VIS-NIR Measurement: Full-scale absorption spectra were measured by the UV–VIS–NIR spectrometer (PerkinElmer, Lambda 1050) ranging from 400 to 1800 nm. The E_G, E_U, and optical loss were obtained from mathematic treatment of α.

Statistical Analysis: All the data presented were from at least three independent experiments and SDs of α are shown as follows: 0.026 cm^{-1} for AJLZ53-0.60@PSM, 0.123 cm^{-1} for AJLZ53–0.94@PSM, 0.035 cm^{-1} for AJLZ53–1.30@PSM, 0.064 cm^{-1} for LPD-80-0.60@PSM, 0.048 cm^{-1} for LPD-80–0.10@PSM, 0.024 cm^{-1} for LPD-80–1.30@PSM, 0.028 cm^{-1} for AJLS102–0.94@PSM, 0.005 cm^{-1} for AJL28–0.94@PSM, 0.075 cm^{-1} for TTE-Ref-0.94@PSM, 0.043 cm^{-1} for EOMG-2–1.00@PSM, 0.079 cm^{-1} for EOMG-1–1.00@PSM, 0.027 cm^{-1} for APTBD-5-1.00@PSM, 0.084 cm^{-1} for F1-0.60@PSM, 0.037 cm^{-1} for M1-0.60@PSM, 0.036 cm^{-1} for M1-ON-0.60@PSM, 0.066 cm^{-1} for M1a-FP-ON-0.60@PSM, 0.084 cm^{-1} for AJLZ53-0.94@COP, 0.081 cm^{-1} for APTBD-5–1.00@COP, and 0.049 cm^{-1} for M1a-FP-ON-0.60@COP. All data were statistically analyzed with Origin.

Supporting Information

Supporting Information is available from the Wiley Online Library or from the author.

Acknowledgements

The authors thank Prof. Guowei Deng at the College of Chemistry and Life Science and Sichuan Provincial Key Laboratory for Structural Optimization and Application of Functional Molecules of Chengdu Normal University (Chengdu 611130, China) for providing chromophore EOMG-1 and EOMG-2 to the study. This work was supported in part by Fundamental Research Project funding from Guangdong-Hong Kong-Macao research team projects of Guangdong Basic and Applied Basic Research Foundation (No. 2020B1515130006), National Natural Science Foundation of China (Nos. U20A20165), Research Grants Council (RGC) of Hong Kong (RGC Ref Nos. 11306320, 11317922, and 11303721), internal research supports or initiatives from City University of Hong Kong (Nos. 7005262, 9680263, and 9610454).

Conflict of Interest

The authors declare no conflict of interest.

Data Availability Statement

The data that support the findings of this study are available in the supplementary material of this article.

Keywords

Monolog-Lorentz (ML) model, optical loss, organic electro-optic material, Tauc method, vibrational overtone

Received: January 31, 2024
Revised: May 7, 2024
Published online: June 7, 2024

[1] D. M. Burland, R. D. Miller, C. A. Walsh, *Chem. Rev.* **1994**, *94*, 31.
[2] S. R. Marder, B. Kippelen, A. K.-Y. Jen, N. Peyghambarian, *Nature.* **1997**, *388*, 845.
[3] L. R. Dalton, P. A. Sullivan, D. H. Bale, *Chem Rev.* **2010**, *110*, 25.
[4] S. Koeber, R. Palmer, M. Lauermann, W. Heni, D. L. Elder, D. Korn, M. Woessner, L. Alloatti, S. Koenig, P. C. Schindler, H. Yu, W. Bogaert, L. R. Dalton, W. Feude, J. Leuthold, C. Koos, *Light Sci. Appl.* **2015**, *4*, e255.
[5] A. Messner, D. Moor, D. Chelladurai, R. Svoboda, J. Smajic, J. Leuthold, *APL Photonics.* **2023**, *8*, 100901.
[6] G. Sinatkas, T. Christopoulos, O. Tsilipakos, E. E. Kriezis, *J. Appl. Phys.* **2021**, *130*, 010901.
[7] J. Wu, Z. Li, J. Luo, A. K.-Y. Jen, *J. Mater. Chem. C.* **2020**, *8*, 15009.
[8] C. Haffner, D. Chelladurai, Y. Fedoryshyn, A. Josten, B. Baeuerle, W. Heni, T. Watanabe, T. Cui, B. Cheng, S. Saha, D. L. Elder, L. R. Dalton, A. Boltasseva, V. M. Shalaev, N. Kinsey, J. Leuthold, *Nature.* **2018**, *556*, 483.
[9] a) Y. Enami, C. T. Derose, D. Mathine, C. Loychik, C. Greenlee, R. A. Norwood, T. Kim, J. Luo, Y. Tian, A. K-Y. Jen, N. Peyghambarian, *Nat. Photonics.* **2007**, *1*, 180; b) T.-D. Kim, J. W. Kang, J. Luo, S. H. Jang, J. W. Ka, S. Hau, Z. Shi, T. Gray, R. M. Overney, J. B. Benedict, A. K.-Y. Jen, *J. Am. Chem. Soc.* **2007**, *129*, 488; c) M. Li, S. Huang, X.-H. Zhou, Y. Zang, J. Wu, Z. Cui, J. Luo, A. K.-Y. Jen, *J. Mater. Chem. C.* **2015**, *3*, 6737.
[10] Z. Zeng, J. Liu, T. Luo, Z. Li, J. Liao, W. Zhang, L. Zhang, F. Liu, *Chem. Sci.* **2022**, *13*, 13393.
[11] X. Liu, P. Tan, X. Ma, D. Wang, X. Jin, Y. Liu, B. Xu, L. Qiao, C. Qiu, B. Wang, W. Zhao, C. Wei, K. Song, H. Guo, X. Li, S. Li, X. Wei, L.-Q. Chen, Z. Xu, F. Li, H. Tian, S. Zhang, *Science.* **2022**, *376*, 371.
[12] L. Zhang, F. Liu, R. Yang, F. Huo, W. Zhang, Y. Zhang, C. Liu, C. Hui, J. W. Hui, *Adv. Sci.* **2023**, *10*, 2304229.
[13] S. Ummethala, T. Harter, K. Koehnle, Z. Li, S. Muehlbrandt, Y. Kutuvantavida, J. Kemal, P. Marin-Palomo, J. Schaefer, A. Tessmann, S. K. Garlapati, A. Bacher, L. Hahn, M. Walther, T. Zwick, S. Randel, W. Freude, C. Koos, *Nat. Photonics.* **2019**, *13*, 519.
[14] J. D. Witmer, T. P. McKenna, P. Arrangoiz-Arriola, R. Van Laer, E. A. Wollack, F. C. Lin, A. K.-Y. Jen, J. Luo, A. H. Safavi-Naeini, *Quantum Sci. Technol.* **2020**, *5*, 034004.
[15] a) S. Takahashi, B. Bhola, A. Yick, W. H. Steier, J. Luo, A. K. Y. Jen, D. Jin, R. Dinu, *J. Light. Technol.* **2009**, *27*, 1045; b) S. Shahin, Mehravar, P. G., N. Peyghambarian, R. A. Norwood, K. Kieu, *Opt. Express.* **2014**, *22*, 30955.
[16] a) Z. Shi, W. Liang, J. Luo, S. Huang, B. M. Polishak, X. Li, T. R. Younkin, B. A. Block, A. K.-Y. Jen, *Chem. Mat.* **2010**, *22*, 5601; b) Z. Shi, J. Luo, S. Huang, B. M. Polishak, X. H. Zhou, S. Liff, T. R. Younkin, B. A. Block, A. K.-Y. Jen, *J. Mater. Chem.* **2012**, *22*, 951.
[17] a) P. Bhasker, J. Norman, J. Bowers, N. Dagli, *J. Lightwave Technol.* **2020**, *38*, 2308; b) Y. Tominari, T. Yamada, T. Kaji, C. Yamada, A.

Otomo, *Jpn. J. Appl. Phys.* **2021**, *60*, 101002; c) Y. Tominari, T. Yamada, T. Kaji, A. Otomo, *IEICE Trans. Electron.* **2023**, *106*, 228.
[18] R. C. Williamson, R. D. Esman, *J. Lightwave Technol.* **2008**, *26*, 1145.
[19] a) M. Zhang, C. Wang, R. Cheng, A. Shams-Ansari, M. Lončar, *Optica.* **2017**, *4*, 1536; b) K. Luke, P. Kharel, C. Reimer, L. He, M. Lončar, M. Zhang, *Opt. Express.* **2020**, *28*, 24452; c) F. Lenzini, S. Kasture, B. Haylock, M. Lobino, *Opt. Express.* **2015**, *23*, 1748.
[20] a) W. Chen, T. Liu, J. Zou, D. Zhang, M. K. Tse, S. W. Tsang, J. Luo, A. K-Y. Jen, *Adv. Mater.* **2024**, *36*, 2306089; b) T. Liu, D. Zhang, M. R. Huqe, W. Wang, J. A. Zapien, S. W. Tsang, J. Luo, *Sci. China-Chem.* **2022**, *65*, 584; c) C. Haffner, W. Heni, D. L. Elder, Y. Fedoryshyn, N. Đorđević, D. Chelladurai, U. Koch, K. Portner, M. Burla, B. Robinson, L. R. Dalton, J. Leuthold, *Opt. Mater. Express.* **2017**, *7*, 2168.
[21] a) R. R. Barto, C. W. Frank, P. V. Bedworth, S. Ermer, R. E. Taylor, *J. Phys. Chem. B.* **2004**, *108*, 8702; b) R. R. Barto, C. W. Frank, P. V. Bedworth, S. Ermer, R. E. Taylor, *J. Chem. Phys.* **2005**, *122*, 234907.
[22] J. Luo, H. Ma, M. Haller, A. K.-Y. Jen, R. R. Barto, *Chem. Commun.* **2002**, *8*, 888.
[23] a) T. Yamada, I. Aoki, C. Yamada, A. Otomo, *Phys. Status Solidi A-Appl. Mat.* **2023**, *220*, 2300242; b) S. Kamada, R. Ueda, C. Yamada, K. Tanaka, T. Yamada, A. Otomo, *Opt. Express.* **2022**, *30*, 19771.
[24] J. Tauc, R. Grigorovici, A. Vancu, *Phys. Status. Solidi. B-Basic Solid State Phys.* **1966**, *15*, 627.
[25] J. Tauc, *Mater. Res. Bull.* **1970**, *5*, 721.
[26] A. R. Zanatta, I. Chambouleyron, *Phys. Rev. B.* **1996**, *53*, 3833.
[27] a) J. A. Guerra, J. R. Angulo, S. Gomez, J. Llamoza, L. M. Montañez, A. Tejada, J. A. Töfflinger, A. Winnacker, R. Weingärtner, *J. Phys. D-Appl. Phys.* **2016**, *49*, 195102. b) J. A. Guerra, A. Tejada, J. A. Töfflinger, R. Grieseler, L. Korte, *J. Phys. D-Appl. Phys.* **2019**, *52*, 105303. c) F. Orapunt, S. K. O'Leary, *Appl. Phys. Lett.* **2004**, *84*, 523.
[28] J. T. Edmond, *Br. J. Appl. Phys.* **1966**, *17*, 979.
[29] K. Lizárraga, L. A. Enrique-Morán, A. Tejada, M. Piñeiro, P. Llontop, E. Serquen, E. Perez, L. Korte, J. A. Guerra, *J. Phys. D: Appl. Phys.* **2023**, *56*, 365106.
[30] a) V. Srikant, D. R. Clarke, *J. Appl. Phys.* **1998**, *83*, 5447. b) W. M. Yim, E. J. Stofko, P. J. Zanzucchi, J. I. Pankove, M. Ettenberg, S. L. Gilbert, *J. Appl. Phys.* **1973**, *44*, 292.
[31] F. L. Martínez, M. Toledano-Luque, J. J. Gandía, J. Cárabe, W. Bohne, J. Röhrich, E. Strub, I. Mártil, *J. Phys. D-Appl. Phys.* **2007**, *40*, 5256.
[32] M. Beaudoin, A. J. G. DeVries, S. R. Johnson, H. Laman, T. Tiedje, *Appl. Phys. Lett.* **1997**, *70*, 3540.
[33] A. Skumanich, C. R. Moylan, *Chem. Phys. Lett.* **1990**, *174*, 139.
[34] M. Halonen, L. Halonen, H. Buerger, P. Moritz, *J. Phys. Chem.* **1992**, *96*, 4225.
[35] O. Ambacher, W. Rieger, P. Ansmann, H. Angerer, T. D. Moustakas, M. Stutzmann, *Solid State Commun.* **1996**, *97*, 365.
[36] W. B. Jackson, N. M. Amer, A. C. Boccara, D. Fournier, *Appl. Optics.* **1981**, *20*, 1333.
[37] A. C. Boccara, D. Fournier, J. Badoz, *Appl. Phys. Lett.* **1980**, *36*, 130.
[38] C. Pitois, A. Hult, D. Wiesmann, *J. Opt. Soc. Am. B-Opt. Phys.* **2001**, *18*, 908.
[39] a) H. Chen, B. Chen, D. Huang, D. Jin, J. Luo, A. K.-Y. Jen, R. Dinu, *Appl. Phys. Lett.* **2008**, *93*, 043507; b) S. Takahashi, B. Bhola, A. Yick, W. H. Steier, J. Luo, A. K.-Y. Jen, D. Jin, R. Dinu, *J. Lightwave Technol.* **2009**, *27*, 1045; c) R. Dinu, D. Jin, G. Yu, B. Chen, D. Huang, H. Chen, A. Barklund, E. Miller, C. Wei, J. Vemagiri, *J. Lightwave Technol.* **2009**, *27*, 1527.
[40] S. J. Ikhmayies, R. N. Ahmad-Bitar, *J. Mater. Res. Technol-JMRT.* **2013**, *2*, 221.
[41] P. Norouzzadeh1, K. Mabhouti, M. M. Golzan1, R. Naderali, *Appl. Phys. A-Mater. Sci. Process.* **2020**, *126*, 1.
[42] R. R. Barto, C. W. Frank, P. V. Bedworth, R. E. Taylor, W. W. Anderson, S. Ermer, A. K.-Y. Jen, J. D. Luo, H. Ma, H.-Z. Tang, M. Lee, A. S. Ren, *Macromolecules* **2006**, *39*, 7566.
[43] J. Zou, D. Zhang, W. Chen, J. Luo, *Mater. Adv.* **2021**, *2*, 2318.
[44] a) D. Zhang, W. Chen, J. Zou, J. Luo, *Chem. Mater.* **2021**, *33*, 3702; b) D. Zhang, J. Zou, W. Chen, S.-M. Yiu, M.-K. Tse, J. Luo, A. K.-Y. Jen, *Chem. Mater.* **2022**, *34*, 3683.
[45] D. Zhang, J. Zou, W. Wang, Q. Yu, G. Deng, J. Wu, Z.-A. Li, J. Luo, *Sci. China-Chem.* **2021**, *64*, 263.
[46] I. Davydenko, S. Benis, S. B. Shiring, J. Simon, R. Sharma, T. G. Allen, S.-H. Chi, Q. Zhang, Y. A. Getmanenko, T. C. Parker, J. W. Perry, J.-L. Brédas, D. J. Hagan, E. W. V. Stryland, S. Barlow, S. R. Marder, *J. Mater. Chem. C.* **2018**, *6*, 3613.

